Research Article | Vol. 27, No. 3 | 4 Feb 2019 | OPTICS EXPRESS 2988
Optics EXPRESS

A novel simulation and analysis algorithm for high resolution optical transition radiation imaging

J. WOLFENDEN,[1,2,*] R. B. FIORITO,[1,2] AND C. P. WELSCH[1,2]

[1] *Cockcroft Institute, Sci-Tech Daresbury, Warrington WA4 4AD, UK*
[2] *School of Physical Sciences, University of Liverpool, Liverpool L69 3BX, UK*
[*] *joseph.wolfenden@cockcroft.ac.uk*

Abstract: The use of optical transition radiation (OTR) for charged particle beam imaging is a well-established and commonly used technique. As such, simulations of the images expected from an arbitrary transverse beam profile are important in both the design of such OTR imaging systems and the analysis of the data. However OTR image simulations of high-energy, low-emittance particle beams, that are becoming commonplace within accelerator physics, can be extremely challenging to produce and limited in their account of practical factors. In this paper we systematically show how high-energy OTR image simulations can be carried out using low-energy parameters, whilst providing little deviation in the resulting transverse beam profiles. Simulations require significantly less resources and can be combined with further analysis techniques, which would otherwise be too costly to be practically viable. Using this methodology as a basis for OTR simulations, we present a new method of analyzing OTR transverse beam profile data for high-energy, low-emittance beams. In contrast to previous work, this algorithm includes the effects of a finite bandwidth and directly allows the inclusion of optical effects, such as chromatic aberration

1. Introduction

Transition radiation is a broadband source of electromagnetic radiation which is produced as a charged particle crosses a boundary between two materials with different dielectric constants [1]. The optical part of this spectrum is known as optical transition radiation (OTR). Due to the direct dependence on beam parameters and the high resolution attainable, OTR is typically used as a diagnostic tool in transverse profile monitors for charged particle beams; especially high-energy electron and proton beams. OTR is produced in both the parallel (forwards) and the anti-parallel (backwards) directions [2]. Most diagnostic applications of OTR imaging use a tilted screen, as this rotates the trajectory of the backward OTR out of the path of the beam, allowing an optical system to collect the radiation [3]. This rotation can produce an asymmetry in an OTR image, but for high-energy beams the asymmetry is negligible [3].

For a single frequency, the OTR image produced is a convolution of the transverse beam profile and the spectral OTR single particle function (SPF) [4]. The spectral OTR SPF is the OTR image produced by a single particle for a single frequency. This is analogous to the point spread function (PSF) [5], which for a given optical system depends on the optical properties of the components of the system [4]. To fully simulate an OTR image the spectral OTR SPF must be integrated over the bandwidth used to perform the imaging, prior to a convolution with the transverse beam distribution [2]. This convolution process provides the potential for a diagnostic method to image low-emittance, low-dispersion beams with sub-micrometer transverse profiles [6], such as those in many Synchrotron Light Sources and Free Electron Lasers (FELs) worldwide, and those proposed at the Compact Linear Collider (CLIC) [7] and the International Linear Collider (ILC) [8]. This method is only applicable to bunch lengths much larger than optical wavelengths;

#349942 https://doi.org/10.1364/OE.27.002988
Journal © 2019 Received 2 Nov 2018; revised 11 Dec 2018; accepted 17 Dec 2018; published 30 Jan 2019

Optics EXPRESS

otherwise coherence effects begin to interfere and dominate the OTR image produced [9].

Current OTR profile measurements usually fit a model for the transverse distribution, e.g. a Gaussian, to the OTR image. This is an adequate methodology for most applications. However, in low-emittance, low-dispersion beams with sub-micrometer transverse sizes, the image cannot be directly linked to the beam profile. The OTR SPF has a double lobe distribution with a characteristic width [4]. As the transverse beam size approaches the width of the OTR SPF the resulting convolution will not accurately reproduce the beam distribution, as the beam distribution will no longer dominate the image. This poses a challenge when using OTR profile monitors for relativistic beams, as the beam profile cannot be directly captured due to the non-trivial structure of the OTR SPF. However, previous work [6] has shown that it is still possible to extract the transverse beam size in this scenario. A ratio known as the visibility has been proven to be directly proportional to the beam size. The visibility is the ratio of the central intensity value of the OTR image and its peak intensity. For the OTR SPF this central intensity value is zero. The visibility has previously been extracted using an empirical formula and a self-calibration technique [6]. We present a methodology to accurately simulate the expected OTR SPF for any imaging system, whilst significantly reducing the computational and temporal requirements typically required. This OTR SPF can be produced in combination with real optical effects, such as a fixed bandwidth, chromatic aberrations, spherical aberrations and even misalignments. Through convolutions with transverse beam distributions, the same results as the empirical approach can not only be achieved, but even surpassed. There is great potential to extend the technique to smaller distributions and a variety of optical systems.

2. Benchmarking Zemax OpticStudio OTR simulations

To simulate the expected OTR SPF it is necessary to know the OTR source electric field distribution. The electric field produced by an electron can be expressed as that of a collection of pseudo-photons [10]. When the electron is at an ultra-relativistic energy, the longitudinal electric field becomes compressed in the direction of propagation, and the remaining transverse fields can be described as a pseudo-photon disc, or a plane wave, with a characteristic width of $\gamma\lambda/2\pi$ [11], where γ is the Lorentz factor and λ is the wavelength of the emitted radiation. This pseudo-photon disc then reflects off the target surface and produces real photons [12]. This analogy with plane waves is a useful tool, as it allows a direct analytical distribution to be derived for the OTR transverse source fields [1, 11, 13, 14],

$$E^{s}_{(x_s,y_s)} = \frac{q\alpha}{(2\pi)^{3/2}\, v\epsilon_0} \frac{(x_s, y_s)}{r_s} K_1(\alpha r_s), \tag{1}$$

where $\alpha = k/\beta\gamma$, k is the wavenumber, v is the particle velocity, $K_1(x)$ is the first-order modified Bessel function of the second kind, q is the particle charge, ϵ_0 is the permittivity of free space, and (x_s, y_s) are spatial co-ordinates upon the source plane, with $r_s = \sqrt{(x_s^2 + y_s^2)}$.

Simulations were carried out using Zemax OpticStudio (ZOS) [15]. This software provides the means to design and analyze many aspects of an optical system. It can propagate the transverse electric fields of any user defined source through the various surfaces of an optical system. The source distribution defined in Eq. (1) was entered into ZOS using a custom Dynamic Link Library (DLL). ZOS operates using a method known as the Slowly Varying Amplitude (SVA) approximation [15], which states that the electric field being propagated must vary slowly in comparison to both the wavelength and mesh size simulated. At the center of Eq. 1 this approximation cannot be justified due to a discontinuity. However it can be shown [16] that this central portion of the source distribution cannot contribute to any image distribution. This can also be thought of in terms of Optical Diffraction Radiation (ODR) where an aperture is used to produce radiation rather than a target. There is no discernible difference between the angular or

Optics EXPRESS

spatial distributions of OTR and ODR when the aperture radius used, R_0, maintains the condition $R_0 << 1/k\theta_M$, where θ_M is the angular field of view of any collection device (e.g. a lens, a detector, etc.); therefore field contributions from within R_0 do not contribute to the measured distribution of OTR [12]. To ZOS this central discontinuity appears as an aperture with a radius defined by the mesh resolution and $<< R_0$. Outside of this central point the SVA approximation holds and ZOS behaves as designed. To ensure the accuracy of the ZOS simulations and the SVA approximation, the spectral intensity produced was compared with that expected from theory. A diagram presenting the schematic used in these comparisons is shown in Fig. 1.

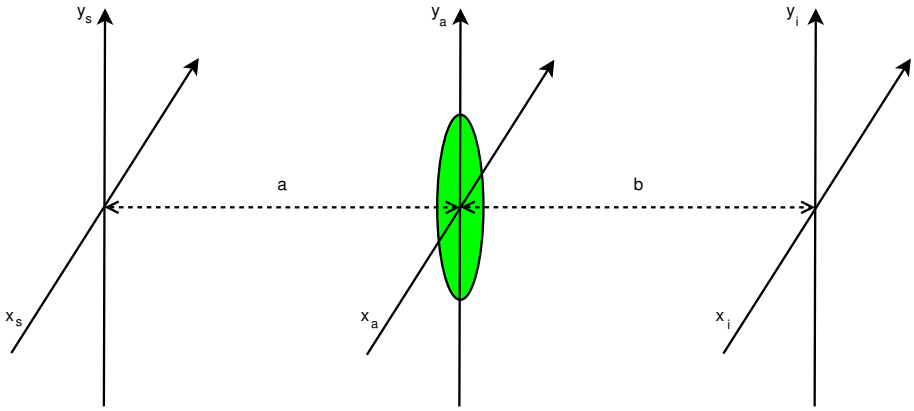

Fig. 1. Diagram representing the simple ideal lens set-up used in both theory and ZOS simulations. a is the object distance and b is the image distance, with $1/f = 1/a + 1/b$ where f is the focal length of the ideal lens. The subscripts s, a and i indicate the plane on the source, the plane at a distance a and the plane on the image respectively.

Spectral OTR angular distributions produced by ZOS and existing theory [2, 11, 17] were the first comparisons. The analytical spectral angular distribution was found by using Fresnel diffraction theory [19] to propagate the source distribution in Eq. (1) a known distance, a. This produces the following electric field distribution,

$$E^a_{(x_a,y_a)} = \frac{-q\alpha}{\sqrt{2\pi}\epsilon_0 v\lambda a} e^{ika} e^{\frac{ik}{2a}r_a^2} \frac{(x_a, y_a)}{r_a} \int_0^\infty dr_s r_s K_1(\alpha r_s) J_1\left(\frac{k r_a r_s}{a}\right) e^{\frac{ik}{2a}r_s^2} \tag{2}$$

where $J_1(x)$ is the first-order Bessel function of the first kind, and (x_a, y_a) are spatial co-ordinates upon the plane at a distance a from the source, with $r_a = \sqrt{(x_a^2 + y_a^2)}$. Various propagation distances were input into Eq. (2) and the intensities produced were directly compared with the output of ZOS simulations. These comparisons are presented in Fig. 2. Both the shape and absolute intensity of the spectral irradiance agreed. The distances are described in terms of the formation length of the OTR, which is defined as $\gamma^2\lambda/2\pi$ [20]. This can be used to quantify the far-field of an OTR source, in that the distance from the source must be much greater than the formation length. Note, the comparisons in Fig. 2 are independent of both energy and frequency. Agreement was also found with existing theory, calculated via alternate analytical methods [17].

Building upon this comparison, the spectral irradiance on the image plane was also benchmarked against theory. The theoretical distribution can be found by further propagation of Eq. (2) and the inclusion of a phase shift due to a focusing element [4, 11, 19]. The analytical form of the

Optics EXPRESS

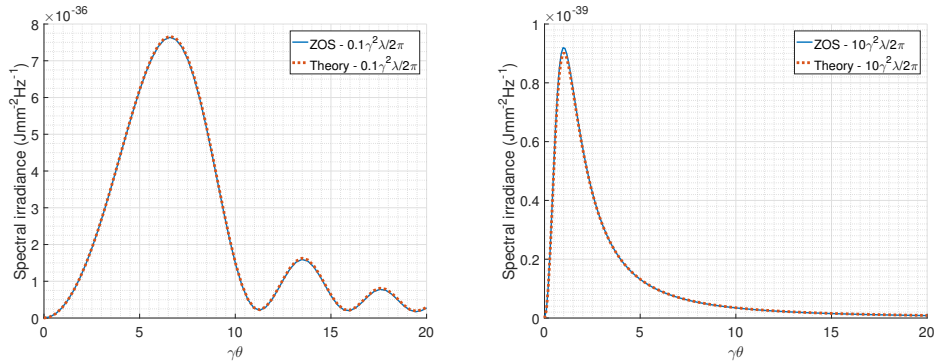

(a) (b)

Fig. 2. Comparison of single electron OTR angular distributions from ZOS and theory. Figure 2a is the comparison of distributions in the near-field. Figure 2b is the comparison of distributions in the far-field. The different distances from the source are in units of $\gamma^2\lambda/2\pi$, the formation length of OTR.

field distribution in the image plane can then be defined as,

$$
\begin{aligned}
E^i_{(x_i,y_i)} &= \frac{\sqrt{2\pi}q\alpha\rho_l}{\nu\lambda^2 ab\epsilon_0} e^{ik(a+b)} e^{\frac{ik}{2b}r_i^2} \frac{(x_i, y_i)}{r_i} f_i(r_s, a, b, \alpha, \rho_l) \\
f_i &= \int_0^\infty dr_s \frac{r_s K_1(\alpha r_s) e^{\frac{ik}{2a}r_s^2}}{\left(\frac{kr_i}{b}\right)^2 - \left(\frac{kr_s}{a}\right)^2} \left[\frac{kr_s}{a} J_1\left(\frac{k\rho_l r_i}{b}\right) J_0\left(\frac{k\rho_l r_s}{a}\right) \right. \\
&\quad \left. - \frac{kr_i}{b} J_0\left(\frac{k\rho_l r_i}{b}\right) J_1\left(\frac{k\rho_l r_s}{a}\right) \right]
\end{aligned}
\tag{3}
$$

where ρ_l is the radius of the ideal lens, $J_0(x)$ zeroth-order Bessel function of the first kind, and (x_i, y_i) are spatial co-ordinates upon the image plane, with $r_i = \sqrt{(x_i^2 + y_i^2)}$. The spectral OTR SPF is then defined as [19],

$$
\frac{d^2U_p(r_i, \nu)}{d\nu dr} = \frac{2}{\mu_0 c}(|E^i_{x_i}|^2 + |E^i_{y_i}|^2), \tag{4}
$$

where ν is frequency and μ_0 is the permeability of free space. The custom DLL was used to benchmark the OTR SPF from a simple ideal lens system, shown in Fig. 1, against the image calculated using Eq. (4). Figure 3 presents this comparison for $a = b = 2f$, $\lambda = 550$nm and an angular acceptance of the lens, θ_m, of 83.3mrad; in principle Eq. (3) can produce a distribution for arbitrary input parameters. These parameters have been used throughout this paper, unless otherwise stated. To the authors knowledge, this is the first time ZOS has been shown to be able to reproduce the image distribution predicted by theory in both shape and absolute intensity.

3. Energy insensitivity in OTR SPF

In practice an OTR target must be larger than several $\gamma\lambda/2\pi$ [18]. This is to accommodate an infinite boundary approximation, preventing diffraction effects interfering with the image distribution. To accurately simulate the OTR source distribution it is also necessary to ensure this infinite boundary approximation is upheld within ZOS. Herein lies the cause of the problem which arises when simulating large γ beams. As the energy of the beam increases, so too must the

Optics EXPRESS

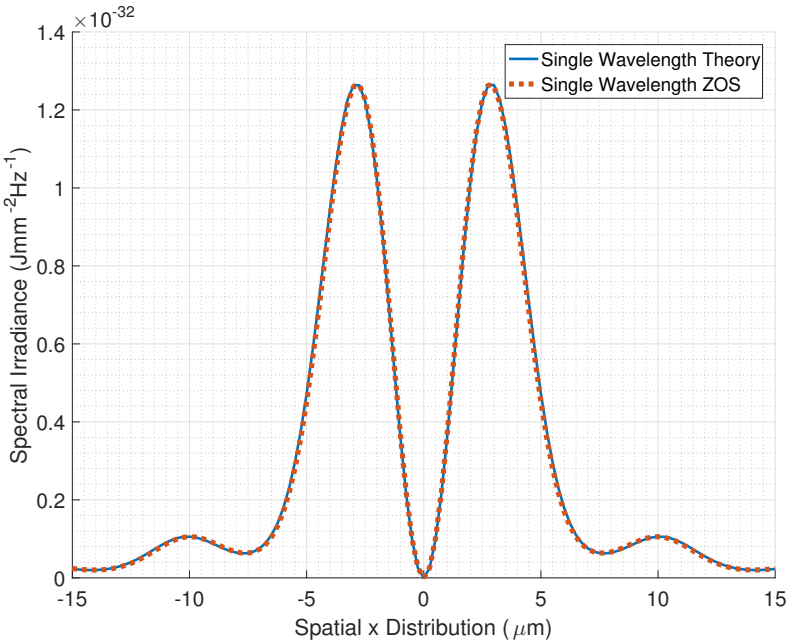

Fig. 3. Comparison of spectral OTR SPF from ZOS and theory. These distributions were produced using λ = 550nm, electron energy E = 300MeV and θ_m = 83.3mrad.

size of the ZOS input grid. To maintain the required resolution across the source, the number of sampling points must also increase. For example, to accurately simulate the OTR SPF produced by the 1.3 GeV (γ = 2544) electron beam at the Accelerator Test Facility 2 (ATF2) at KEK (Japan), a sampling of 65536x65536 is required [18]. This leads to large requirements of both computational power and time; the above parameters would require 350GB of RAM per surface propagation (e.g. each singlet lens consists of two surfaces) [15].

However, the angular distribution of OTR points towards a method of reducing these stringent requirements. In most applications OTR imaging systems cannot be placed in the far-field. For GeV beams this is of the order of metres. From Fig. 2a it is clear that, even in the extreme near-field, the majority of the intensity is confined to within a field of view less than $10/\gamma$, and as the distance from the source increases, this field of view decreases. Therefore, if $\theta_m > 10/\gamma$ the majority of the wavefront of the OTR distribution will be captured. There is little benefit in increasing the field of view further, as little additional information is collected. By this logic, for a fixed angular field of view, if γ is increased to the point that $\theta_m > 10/\gamma$, there is no difference found in the resulting image distribution for larger γ. Previously this argument has been explored mathematically [4], but to our knowledge the physical mechanism behind it has never been elaborated upon.

To demonstrate this concept Fig. 4 compares the spectral OTR SPF, calculated using Eq. (4), for a high energy electron and a lower energy electron. It is evident that the differences between the two distributions are minimal overall; there is a $< 1\%$ error in the peak intensity produced and no change in the position of the peaks. Reducing γ directly reduces the effective source size. This is turn directly reduces the required simulation grid size and sampling, making the simulation process more computationally efficient and much quicker. Consequently, the simulation results can be used for more elaborate analysis, such as bandwidth effects which require multiple simulations of the same system for a range of wavelengths.

Optics EXPRESS

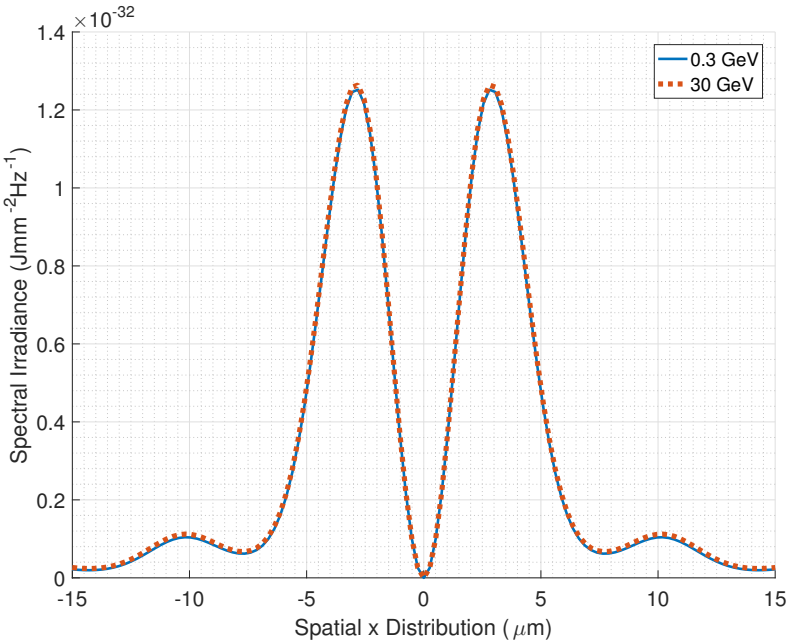

Fig. 4. Comparison of the OTR SPF from an ideal lens imaging system, for a 30 GeV electron and a 0.3 GeV electron.

4. Bandwidth and beam size effects

One of the main assumptions of an OTR source distribution is that the target the electron is incident upon is infinite in extent. In reality, as previously described, the target dimensions should be much larger than $\gamma\lambda/2\pi$. This has the additional benefit that the specific transverse position where the electron interacts with the target surface does not affect the source distribution. This means that the effect of beam size on the OTR SPF can be included by a simple convolution [4],

$$\frac{dU_b(r_i)}{dr_i} = \int_{-\infty}^{\infty} S(r_i)\frac{dU_p(r_i-\tau)}{dr_i}d\tau, \tag{5}$$

where $\frac{dU_b(r_i)}{dr_i}$ is the resultant OTR image of the beam, $S(r)$ is the transverse beam distribution and $\frac{dU_p(r_i)}{dr_i}$ is the OTR SPF intensity distribution. This OTR SPF is calculated by integrating Eq. (4) over the required frequency bandwidth,

$$\frac{dU_p(r_i)}{dr} = \int_{\Delta\nu} T(\nu)\frac{d^2U_p(r_i,\nu)}{d\nu dr}d\nu, \tag{6}$$

where $T(\nu)$ is the transmission response of the bandwidth filter and $\Delta\nu$ is the frequency bandwidth. Equation (6) can be used to account for many experimental frequency effects, such as a bandwidth filter transmission curve or the quantum efficiency of a camera.

It is critical that any simulations run at lower energies do not contaminate the expected visibility of the higher energy result; as previously stated, this is directly dependent upon the transverse beam size. Figure 5 is a comparison of the distributions from Fig. 4 integrated over a 40nm flat-top bandwidth, and convoluted with a Gaussian transverse beam distribution with a 0.5μm width and a 1nC bunch charge; typical parameters for facilities where this measurement would

Optics EXPRESS

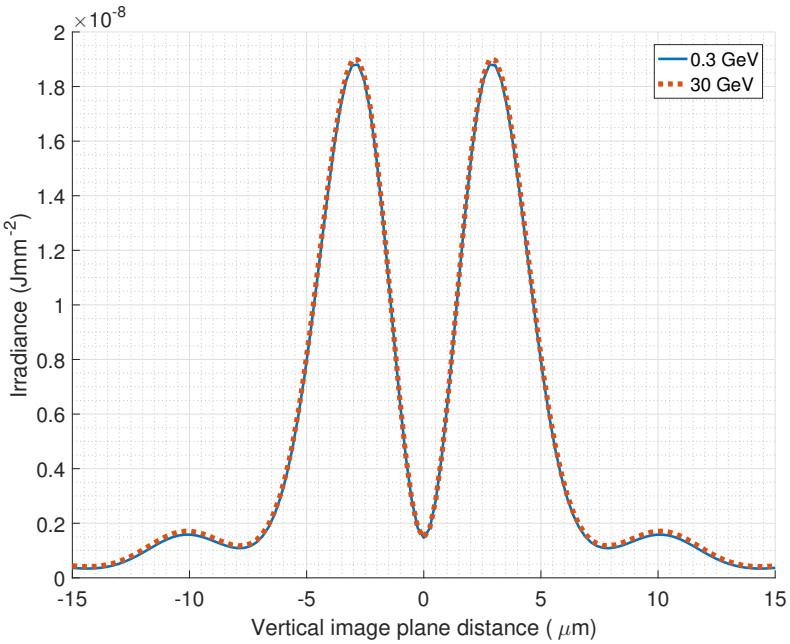

Fig. 5. Comparison of an OTR image of a 1nC, 0.5μm Gaussian beam from an ideal imaging system with a 40nm flat-top bandwidth, for 30 GeV and 0.3 GeV electrons.

be of interest [6]. The visibility difference between the two distributions is 0.1%, which directly translates to an equivalent error of 0.1% in the beam size produced, well within acceptable limits of traditional methods. Figure 5 also represents the first ZOS-based simulation to produce the absolute intensity expected by a single bunch of charged particles for a specific bandwidth and transverse profile.

To further investigate the effect of beam energy on the image visibility, the percentage variation in the expected visibility of a high energy beam image was calculated as a function of the actual simulation energy. As a demonstration of the impact of this effect, parameters similar to those quoted earlier used in previous work were chosen (1.3 GeV (γ = 2544) used at ATF2). Figure 6 shows that the percentage variation is < 1% for $\gamma > 300$. It follows that OTR simulations for $\gamma > 300$ can be carried out with $\gamma = 300$ with minimal error introduced to the resulting beam size. For $\gamma < 300$ the error is no longer negligible, but at these energies the OTR simulations are trivial, as the source distribution is sufficiently small to allow low sampling to be used. Therefore, previous simulations carried out using sampling of 65536x65536, leading to memory requirements of 350GB per surface, could be completed using 2048x2048 and only 600MB per surface; a substantial gain in both computational time and resources.

5. Beam size analysis algorithm

A novel analysis algorithm for OTR images of low-emittance, low-dispersion electron beams has been designed using the simulation methodologies described above. The crucial components of this algorithm are the ability of ZOS to simulate real lenses and the inclusion of chromatic effects from a finite bandwidth.

ZOS contains a library of stock optical components from a range of manufacturers, but it also holds the ability to design custom optical components. This means that optical systems can

Optics EXPRESS

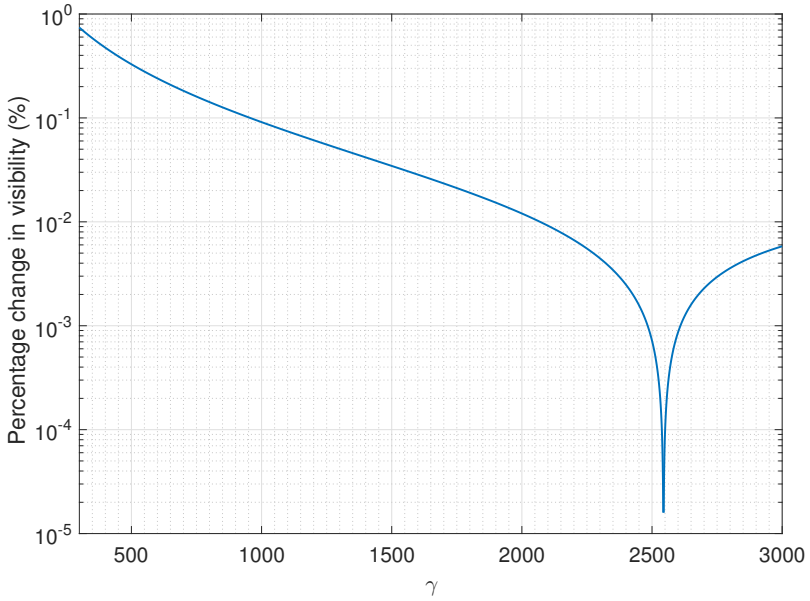

Fig. 6. The percentage variation with energy in the visibility produced in an OTR image by a 0.5μm Gaussian electron beam, in comparison to an energy of 1.3GeV (γ = 2544). Produced using Eq. (4).

be directly reproduced for simulation purposes, including all the aberrations associated with the physical system. In addition to including real lens effects, ZOS can also include optical components such as vacuum windows, filters and polarizers, all of which can affect the final image. Combining all these components enables a simulation to be carried out which contains all the aberrations one would expect to find in a physical system.

By appropriately leveraging the energy independence of the OTR SPF, an increased simulation efficiency allows more elaborate analyses to be undertaken that, until now, have otherwise been impractical. One such analysis is the inclusion of chromatic aberrations created by using a bandwidth. ZOS simulations can be run repeatedly for a range of wavelengths spanning a bandwidth, before numerically calculating Eq. (6).

As single wavelength results are often used, these chromatic effects are often ignored. Figure 7 is a comparison of the ZOS simulated image of a 3μm Gaussian electron beam for a single wavelength, with a 40nm flat-top bandwidth, and with a 100nm flat-top bandwidth. The distributions have been normalised to aid comparison. The obvious differences between the distributions exemplify why the effect of bandwidth is crucially important to include in any OTR simulation. There is a clear difference in the central minimum values of the distributions, which directly translates into a difference in the visibility produced; for 40nm this a 12.5% error, for 100nm this a 57.7% error. From an analysis perspective, this is unacceptable. From a design perspective, this could lead to the assumption of an achievable beam size resolution, which in reality would be unattainable. Alternatively, a wider bandwidth can be intentionally used to obtain an increased signal-to-noise ratio. The visibility error will obviously be larger, however this can now be accounted for with the analysis algorithm; therefore the benefit of high signal-to-noise can be realized.

A detail to note in Fig. 7 is that the peak-to-peak distance decreases as bandwidth increases. This effect is caused by two properties of the spectral OTR SPF. As the wavelength increases, the

Optics EXPRESS

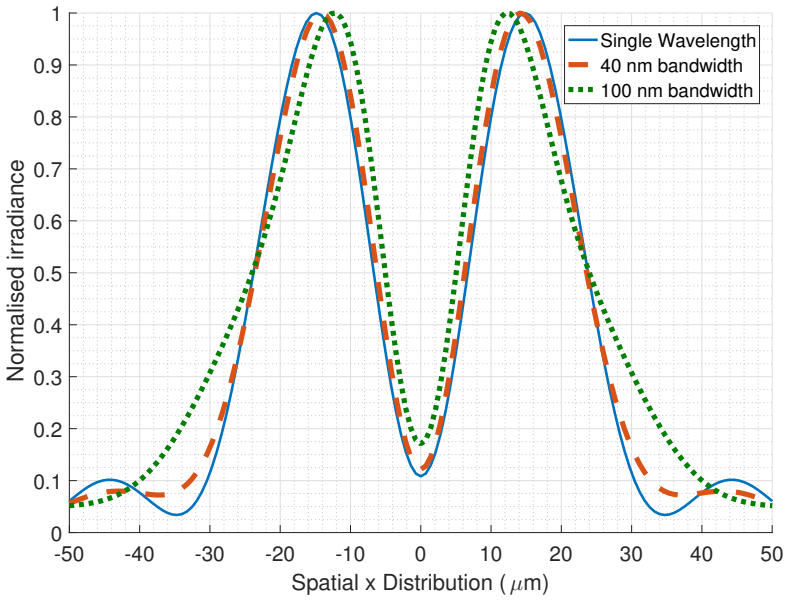

Fig. 7. Comparison of ZOS results for single wavelength and bandwidth simulations of a 3μm transverse beam using a singlet lens (Thorlabs - LA1050-A-ML [21]).

peak-to-peak distance increases and the peak intensity decreases. The combination of these two properties in Eq. (6) leads to the decrease in peak-to-peak distance with increasing bandwidth. For OTR beam size measurements the peak-to-peak distance is a measure of sensitivity; the smaller the distance the greater the sensitivity to changes in beam size [6]. Therefore a larger bandwidth could lead a system to an increased beam size sensitivity. However, it is critical that the visibility change can be attributed to the beam size and not the bandwidth. This algorithm is capable of this distinction.

The analysis algorithm can be described as a three-step process, a diagram of which is presented in Fig. 8. The first step is the definition of the single particle, single frequency source distribution. Note, this paper has focused on the application of this algorithm to OTR, but in principle any beam related radiation source distribution could be entered at this point. For the case of OTR, the source field has the input parameter of energy. This source is then propagated through a pre-defined imaging system in ZOS at a fixed wavelength, producing a simulated spectral OTR SPF. This simulation is carried out multiple times for a range of wavelengths to calculate the OTR SPF for a specified bandwidth, $\Delta\lambda$. The final step is then to convolve this OTR SPF with a transverse profile model with a specified size, σ. These results could then be used to design an optimum system, or the parameters of the beam distribution could be varied and optimized to match experimental data to determine the beam size.

6. Discussion

The use of an innovative technique in simulating OTR SPFs has been demonstrated. Lower energy simulation techniques can be used to reproduce much higher energy results, in both shape and absolute intensity, whilst only introducing negligible error in the resulting images. The combination of this methodology with a full optical system analysis algorithm, that includes bandwidth effects, provides a new process to retrieve transverse beam distributions from OTR

Optics EXPRESS

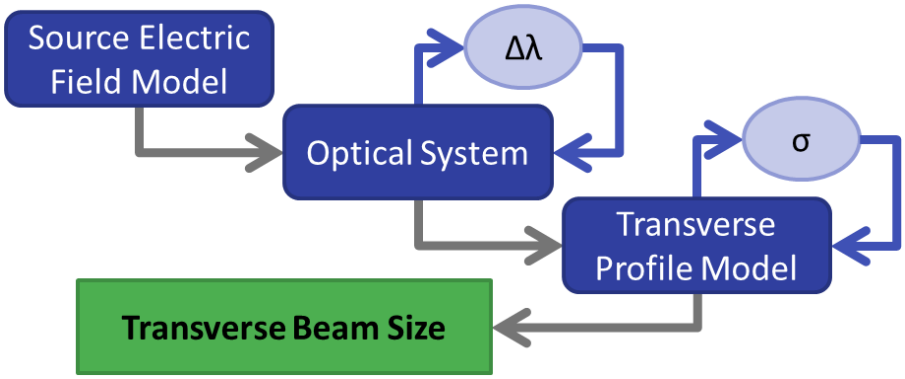

Fig. 8. Flowchart depicting the processes followed throughout the OTR analysis algorithm. $\Delta\lambda$ is the bandwidth used and σ is the transverse beam size entered into the transverse profile model.

images. This is especially pertinent for low-dispersion, low-emittance beams, where current techniques would fail.

This algorithm can also be used to design new imaging systems. It would account for all possible optical aberrations and provide a means to optimize the beam size resolution required for a particular application. The modular design of the algorithm means that each step is independent of the others. The only assumption is that the convolution described in Eq. (5) holds, which is true for all transition radiation produced by low-dispersion beams. Beams with high-dispersion contain particles with a large amount of transverse motion. This transverse motion adds an additional angular component to each individual OTR SPF, effectively smearing out the nominal double-lobe structure and removing the visibility as a measure of beam size. However, any source distribution which follows Eq. (5) could be used as an input. This can then be propagated through any optical system which can be defined in ZOS, accounting for any bandwidth filter used. Then finally, any transverse beam distribution can be convoluted with the result of the ZOS simulation. This process could essentially eliminate the resolution limitation imposed by typical optical techniques.

Sources such as diffraction radiation do not abide by Eq. (5), as the SPF is dependent upon the transverse position of the particle with respect to the center of the target [22]. As stated above, this is also true of non-zero dispersion beams. This limitation could be overcome by replacing the convolution step of the algorithm with a step similar to the ZOS bandwidth analysis. The ZOS simulation can be run for multiple transverse spatial and angular starting positions on the target plane; by summing these results, an effective convolution is performed [23]. Diffraction radiation however introduces an additional energy dependence through the dimensions of the radiator target. This limits the applicability of any high energy simulations using low energy parameters.

Regardless of the limitations in certain parameter spaces, the possibilities provided by this algorithm are applicable to multiple areas of optical diagnostic research. The application of the algorithm to benchmarked OTR data is currently under investigation, along with an adaptation for coherent radiation sources. For coherent transition radiation the source bunch is much smaller than effective field size, $\gamma\lambda/2\pi$, and the emitted wavelengths are comparable or larger than the bunch length; therefore the images produced are completely dominated by the diffraction limited SPF. It would be a straightforward procedure to integrate elements of this incoherent analysis into existing coherent analysis methods (e.g. [9]). This would account for the properties of an optical system in the analysis and subsequent results.

Optics EXPRESS

The applicability and flexibility of this analysis methodology holds great potential for any accelerator or facility operating with low-emittance: e.g. 3^{rd} and 4^{th} generation Synchrotron Light Sources, FELs and future high energy linear colliders.

Funding

This work was supported by the EU under Grant Agreement No. 624890 and the STFC Cockcroft Institute Core Grant No. ST/G008248/1.

Acknowledgments

The authors would like to thank T. Lefevre, S. Mazzoni, R. Kieffer and M. Bergamaschi of the Beam Diagnostics group at CERN, P. Karataev of the JAI at RHUL, and K. Kruchinin of Eli-Beamlines for many helpful discussions on this topic.

Disclosures

The authors declare that there are no conflicts of interest related to this article.

References

1. M. L. Ter-Mikaelian, *High Energy Electromagnetic Processes in Condensed Media* (Wiley-Interscience, 1972).
2. A. G. Shkvarunets and R. B. Fiorito, "Vector electromagnetic theory of transition and diffraction radiation with application to the measurement of longitudinal bunch size," Phys. Rev. ST Accel. Beams **11**, 012801 (2008).
3. A. Potylitsyn, "Transition radiation and diffraction radiation. Similarities and differences," Nucl. Instrum. Methods. Phys. Res. B **145**, 169–179 (1998).
4. D. Xiang and W. H. Huang, "Theoretical considerations on imaging of micron size electron beam with optical transition radiation," Nucl. Instrum. Methods. Phys. Res. A **570**, 357–364 (2007).
5. E. Hecht, *Optics* (Addison Wesley, 1987), 2nd ed.
6. K. Kruchinin, A. Aryshev, P. Karataev, B. Bolzon, T. Lefevre, S. Mazzoni, M. Shevelev, S. T. Boogert, L. J. Nevay, N. Terunuma, and J. Urakawa, "Sub-micrometer transverse beam size diagnostics using optical transition radiation," J. Phys. Conf. Ser. **517**, 012011 (2014).
7. M. Aicheler, P. Burrows, M. Draper, T. Garvey, P. Lebrun, K. Peach, N. Phinney, H. Schmickler, D. Schulte, and N. Toge, "A Multi-TeV linear collider based on CLIC technology: CLIC Conceptual Design Report," Tech. rep. (2012).
8. C. Adolphsen, M. Barone, B. Barish, K. Buesser, P. Burrows, J. Carwardine, J. Clark, H. M. Durand, G. Dugan, E. Elsen, A. Enomoto, B. Foster, S. Fukuda, W. Gai, M. Gastal, R. Geng, C. Ginsburg, S. Guiducci, M. Harrison, H. Hayano, K. Kershaw, K. Kubo, V. Kuchler, B. List, W. Liu, S. Michizono, C. Nantista, J. Osborne, M. Palmer, J. M. Paterson, T. Peterson, N. Phinney, P. Pierini, M. Ross, D. Rubin, A. Seryi, J. Sheppard, N. Solyak, S. Stapnes, T. Tauchi, N. Toge, N. Walker, A. Yamamoto, and K. Yokoya, "The International Linear Collider: Technical Design Report, Volume 3.II: Accelerator Baseline Design," Tech. rep. (2013).
9. H. Loos, R. Akre, A. Brachmann, F.-J. Decker, Y. Ding, D. Dowell, P. Emma, J. Frisch, S. Gilevich, G. Hays, Ph. Hering, Z. Huang, R. Iverson, C. Limborg-Deprey, A. Miahnahri, S. Molloy, H.-D. Nuhn, J. Turner, J. Welch, W. White, J. Wu, and D. Ratner "Observation of Coherent Optical Transition Radiation in the LCLS Linac," in *Proceedings of the 30th International Free Electron Laser Conference,* Gyeongju, Korea, 24-29 Aug. 2008.
10. D. Karlovets and A. Potylitsyn, "Transition radiation in the pre-wave zone for an oblique incidence of a particle on the flat target," Nucl. Instrum. Methods. Phys. Res. B **266**, 3738–3743 (2008).
11. G. Kube, "Imaging with Optical Transition Radiation , Transverse Beam Diagnostics for the XFEL," DESY Report: TESLA-FEL 2008-01, (2008).
12. D. Xiang, W.-H. Huang, and Y.-Z. Lin, "Imaging of high-energy electron beam profile with optical diffraction radiation," Phys. Rev. ST Accel. Beams **10**, 062801, 1–12 (2007).
13. J. D. Jackson, *Classical Electrodynamics* (John Wiley and Sons, 1998), 3rd ed.
14. S. Casalbuoni, B. Schmidt, P. Schmüser, V. Arsov and S. Wesch, "Ultrabroadband terahertz source and beamline based on coherent transition radiation," Phys. Rev. ST Accel. Beams **12**, 030705, 1–13 (2009).
15. Radiant ZEMAX, *Zemax OpticStudio 16.5, User's Manual* (2017).
16. M. Castellano, A. Cianchi, G. Orlandi, and V. A. Verzilov, "Effects of diffraction and target finite size on coherent transition radiation spectra in bunch length measurements," Nucl. Instrum. Methods Phys. Res. A **435**, 297–307 (1999).
17. V. Verzilov, "Transition radiation in the pre-wave zone," Phys. Lett. A **273**, 135–140 (2000).
18. B. Bolzon, A. Aryshev, T. Aumeyr, S. Boogert, P. Karataev, K. Kruchinin, T. Lefevre, S. Mazzoni, L. Nevay, M. Shevelev, N. Terunuma, J. Urakawa, and C. Welsch, "Very high resolution optical transition radiation imaging system: Comparison between simulation and experiment," Phys. Rev. ST Accel. Beams **18**, 082803 (2015).

Optics EXPRESS

19. M. Born and E. Wolf, *Principles of Optics* (Pergamon, 1975), 5th ed.
20. V. Ginzburg and V. Tsytovich, "Several problems of the theory of transition radiation and transition scattering," Phys. Rep. **49**, 1–89 (1979).
21. Thorlabs, "Supplier of optics and opto-mechanical equipment,"www.thorlabs.com.
22. R. Kieffer, E. Bravin, T. Lefevre, S. Mazzoni, M. Bergamaschi, P. Karataev, K. Kruchinin, M. Billing, J. Conway, J. Shanks, N. Terunuma, and L. Bobb, "Optical diffraction radiation for position monitoring of charged particle beams," Nucl. Instrum. Methods. Phys. Res. B **402**, 88–91 (2017).
23. F. G. Bisesto, M. Castellano, E. Chiadroni, and A. Cianchi, "Zemax simulations describing collective effects in transition and diffraction radiation," Opt. Express **26**, 5075–5082 (2018).